International Journal of Plasticity 41 (2013) 53–64

Contents lists available at SciVerse ScienceDirect

International Journal of Plasticity

journal homepage: www.elsevier.com/locate/ijplas

Nanoscale room temperature creep of nanocrystalline nickel pillars at low stresses

In-Chul Choi [a], Yong-Jae Kim [a], Moo-Young Seok [a], Byung-Gil Yoo [a], Ju-Young Kim [b], Yinmin Wang [c], Jae-il Jang [a,*]

[a] Division of Materials Science and Engineering, Hanyang University, Seoul 133-791, Republic of Korea
[b] School of Mechanical and Advanced Materials Engineering, UNIST, Ulsan 689-798, Republic of Korea
[c] Physical and Life Sciences Directorate, Lawrence Livermore National Laboratory, Livermore, CA 94550, USA

ARTICLE INFO

Article history:
Received 5 June 2012
Received in final revised form 25 August 2012
Available online 7 September 2012

Keywords:
Nanocrystalline nickel
Time-dependent plasticity
Nanomechanical properties
Size effect
Creep

ABSTRACT

Nanoscale time-dependent plastic deformation (creep) behavior of nanocrystalline (nc) Ni, at low stresses and at room temperature, was systematically explored through uniaxial creep experiments performed on nano-/micro-pillars (with diameters of 600, 1000, and 2000 nm). It was revealed that the creep indeed occurs at ambient temperature, and exhibits a creep strain of $\sim 2 \times 10^{-4}$–9×10^{-3} (for 200 s load-holding) at stresses below the nominal yield strengths of the pillars. At a given stress, much higher total creep strains and strain rates accrue in the smaller pillars, which is likely due to the increased contributions of free surfaces. Estimation of the stress exponent and the activation volume suggests that the nanoscale creep event under low stresses may be dominated by diffusion-controlled mechanisms such as free surface assisted grain-boundary diffusion and grain-boundary sliding.

1. Introduction

Over the past two decades, appealing mechanical properties of nanocrystalline (nc) metals and alloys (such as ultrahigh strength, enhanced fracture toughness, and excellent wear resistance) have gathered numerous scientific and technological interests, as reviewed in many articles (Barai and Weng, 2009; Benkassem et al., 2007; Capolungo et al., 2007; Cleri, 2012; Dao et al., 2007; Farrokh and Khan, 2009; Gusev, 1998; Han et al., 2005; Khan et al., 2006; Kumar et al., 2003a; Li and Weng, 2007; Malygin, 2007; Meredith and Khan, 2012; Meyer et al., 2006; Ovid'ko, 2005; Suryanarayana, 2005; Tjong and Chen, 2004; Tucker and McDowell, 2011; Valiev et al., 2000; Valiev, 2004; Wang et al., 2012b; Wolf et al., 2005; Zhu and Li, 2010; Zhu and Lu, 2012). One important mechanical property of the materials is the time-dependent plasticity, i.e., creep or visco-plasticity, that is often described by (Dieter, 1988; Kassner and Pérez-Prado, 2004; Sherby and Wadsworth, 1989; Wadsworth et al., 2002):

$$\dot{\varepsilon} = \frac{ADGb}{kT}\left(\frac{b}{d}\right)^{p}\left(\frac{\sigma}{G}\right)^{n} \tag{1}$$

where $\dot{\varepsilon}$ is the steady-state creep rate, A is a dimensionless constant, D is the diffusion coefficient, G is the shear modulus, b is the magnitude of Burgers vector, k is the Boltzmann constant, T is the absolute temperature, d is the grain size, σ is the creep stress, p is the inverse grain size exponent, and n is the creep stress exponent. It has been reported that nc materials can

* Corresponding author.
E-mail address: jijang@hanyang.ac.kr (J.-i. Jang).

0749-6419/$ - see front matter © 2012 Elsevier Ltd. All rights reserved.
http://dx.doi.org/10.1016/j.ijplas.2012.08.008

exhibit creep behavior even at ambient temperature, mainly due to their very high fraction of grain boundaries (and triple junctions) that act as effective diffusion path and strong source/sink of dislocations (Chen et al., 2003; Gianola et al., 2006; Kottada and Chokshi, 2005; Kumar et al., 2003b; McFadden et al., 1999; Rupert et al., 2009; Shan et al., 2004; Van Swygenhoven et al., 2002a; Wang et al., 1997; Zhang et al., 2004).

Recently, the mechanical behavior of nc-materials at the nanoscale has emerged as an interesting research direction. In addition to fundamental scientific relevance, the combined effects of both grain size and deformation volume size on mechanical characteristics in nc materials have technological importance in their possible applications to small-scale structures including the components of micro-electromechnical systems or MEMS (Baghbanan et al., 2006; Gruen, 1999; Tjong and Chen, 2004; Wang et al., 2002). From the engineering viewpoint, the knowledge for time-dependent plasticity at ambient temperature is essential for reliable operating and life-time prediction of such nc-material-based components; but the room temperature (RT) creep behavior of nc-materials at the nanoscale has not been fully investigated.

The time-dependent deformation behavior of nc-materials has been analyzed through various experiments such as tensile/compression (Blum and Li, 2007; Dalla Torre et al., 2002, 2005; Gu et al., 2007; Kottada and Chokshi, 2005; Li et al., 2007; Pan et al., 2007; Prasad and Chokshi, 2010; Shen et al., 2008; Wang and Ma, 2004; Wang et al., 1997, 2006, 2010; Yin et al., 2001) and nanoindentation (Choi et al., 2011; Gu et al., 2007; Ma et al., 2008a, 2008b; Maier et al., 2011; Schwaiger et al., 2003; Wang et al., 2009, 2010) or simulations including finite element analysis and molecular dynamics (Van Swygenhoven, 2002b; Yamakov et al., 2004). Among the methods, nanoindentation creep test (for example, see Choi et al., 2011, 2012; LaFontaine et al., 1990; Lucas and Oliver, 1999; Ma et al., 2008a,b; Mayo and Nix, 1988; Mayo et al., 1990; Yoo et al., 2010a,b) may be the most popular for nano-/micro-scale creep characterization due to many advantages; i.e., testing procedure is simple and easy to set up, and only a small volume of material is needed. Although there are many different types of nanoindentation creep testing methods such as constant displacement test (LaFontaine et al., 1990), constant loading rate test (Mayo and Nix, 1988), and constant strain rate test (Lucas and Oliver, 1999), the most popular method is constant load test (Mayo et al., 1990) using a sharp indenter like a three-sided pyramidal Berkovich indenter having a centerline-to-face angle of 65.3°. However, some critical difference in data between indentation creep and uniaxial creep has been reported; e.g., the values of creep stress exponent, n of Eq. (1) (which can be a valuable indicator for creep mechanism) estimated by the constant-load indentation creep experiments have been much higher than the values from the uniaxial creep test (Choi et al., 2011; Ma et al., 2008a,b), which makes it difficult to judge whether the nanoindentation creep tests provide reliable values or not.

There are many possible reasons for the difference in the quantitative data between uniaxial creep and nanoindentation creep, and they can be categorized into two groups (Choi et al., 2012). First of all, there can be some reasons associated with self-similar geometry of a sharp tip: For example, according to classic contact mechanics, an indentation with a given sharp tip exhibits unique indentation strain ($\varepsilon_i = 0.2\tan\beta$, where β is the inclination of the indenter face to the sample surface (Johnson, 1985)) and stress that are virtually unchanged during indentation creep test. Additionally, the difficulty in applying low stress below the yield strength (if the tip is not blunted) and the presence of indentation size effect (ISE, which is manifested as an increase in hardness with decreasing indentation depth for a sharp indentation; see the review by Pharr et al., 2010) also complicate the creep analysis. In our previous nanoindentation creep study on nc-Ni (Choi et al., 2011), we reported that these sharp-tip related issues can be overcome by adopting a spherical indenter instead of a Berkovich tip.

However, there are still second, and more fundamental, reasons causing the difference in data between nanoindentation creep and conventional uniaxial creep (Choi et al., 2012); the stress state underneath the indenter is much more complicated than uniaxial stress condition in the conventional uniaxial creep tests. Also, it is noteworthy that the proportionality 'constants' for relating hardness H to stress σ and the contact area A to square indentation depth h^2 may not be constant and be seriously affected by hardness-to-modulus (H/E) ratio which changes during creep (Stone et al., 2010). In an attempt to solve these fundamental issues, here we performed uniaxial compression creep tests at RT and under low stresses (<the nominal yield stress) with nano-/micro-pillar sample of nc-Ni. Note that Wang et al. (Wang et al., 2010) conducted some early work of pillar creep test, but their testing conditions were limited to a high temperature (398 K) and a specific load (5 mN that corresponds to ~1.6 GPa) and pillar size (diameter d = 2000 nm). In the present study, through a series of experiments on various-sized pillars under different low stresses (well below the yield strength of the pillars), we systematically explore the RT creep behavior of nc-Ni in terms of the nanoscale creep mechanisms and the size effect on creep.

2. Experimental details

The used material was electrodeposited nc-Ni foil of 150 μm thickness with an average grain size of 30 nm (Wang et al., 2006). Micro-/nanopillars having three different diameters (~600, 1000, and 2000 nm) were fabricated through the focused ion beam (FIB) milling with a Nova 200 NanoLab (FEI Co., Hillsboro, OR, USA) following the method described by Kim and Greer (2009). More than 20 pillars for each diameter were fabricated by top-down ion beam patterning with the final ion current of 10 pA and at a constant ion accelerating voltage of 30 kV. The pillars were made to reside at the center of a 50 μm crater, which provides enough space for the indenter to come down on the sample during the test without contacting the crater rim. The aspect ratio in all pillars was maintained at ~2–3 so that the relative contributions from friction and constraint at the ends of pillars remain constant.

Time-dependent deformation experiments were performed using the Nanoindenter-XP (Agilent Corp., Oak Ridge, TN, USA) with a FIB-milled cylindrical diamond punch whose top diameter is ~14 μm. A major issue while conducting creep

experiments with a nanoindenter is the thermal drift. To avoid any possible experimental artifacts associated with it, thermal drift was maintained below 0.05 nm/s. Prior to the creep segment, a preload was applied (the applied stress is the same as the applied creep stress) so as to minimize the effects of the rounded top surface (i.e., the partly rounded top of a pillar can be flattened even by applying low loads due to the influence of local stress concentration; see Yoo et al., 2012) or possible misalignment of the pillars. During the creep test, the load was increased up to the desired maximum stress level (i.e., 400, 600, 800, 1000 MPa, respectively) at a fixed loading rate, $(dP/dt)/P = 0.05$ /s, then held for 200 s, and finally removed at the same rate as the loading segment. The holding time was chosen in consideration of the thermal and the instrumental drift (Yoo et al., 2010a). More than three tests were conducted for each testing condition, to insure the reproducibility of our results and minimize the effects of possible misalignment (and related friction). Morphology of each pillar was imaged before and after creep test using scanning electron microscopy (SEM), JSM-6330F (JEOL Ltd., Tokyo, Japan).

3. Results

3.1. SEM images

Fig. 1 shows typical SEM micrographs of the pillars taken before and after the creep experiments conducted at a stress of 1000 MPa, the highest stress level of creep experiments in the present study. An inevitable consequence of utilizing the top-down FIB fabrication procedure is that all pillars have a small amount of vertical taper, on the order of ~3°. However, in these pillars, the top-down FIB fabrication has obvious merits since it minimized FIB-induced surface damage because the sidewalls of the pillars are exposed to the ion beam only at the glancing angle. Additionally, diameters of the pillars in this study of 600, 1000, and 2000 nm are relatively larger than those of previous work down to 100 nm (Jang and Greer, 2011) so that effects of tapering geometry or FIB-induced surface damage on size effect could be minimized. It is also noteworthy that, very recently, Schwaiger et al. (2012), who simulated microcompression of ultrafine-grained Ni pillars (with or without taper), reported that the effect of the taper on the load-displacement behavior is relatively small in the elastic regime vis-à-vis the plastic regime. Since the applied stress in our work is below the yield strength, one may expect that the taper effect is not so pronounced and may not change the main results of this work.

As seen in Fig. 1, in all pillars, almost uniform deformation was observed (without shearing, bending, or barreling), which indicates that the creep deformation may be accommodated by the whole body of the pillar, in contrast to the inhomogeneous slips detected in single crystalline metals (Greer et al., 2005; Uchic et al., 2004).

Note that the 'orange peel'- or 'fish skin'-like surface of the pillars in Fig. 1 is generally observed in nanocrystalline pillars that do not exhibit a smooth surface (like single crystal pillars) due to the different energy state of the matrix and grain boundaries. An intriguing feature in Fig. 1 is the phenomenon is more pronounced in crept sample than in non-crept sample (that was only pre-loaded for minimizing artifact). This indicates grain boundary sliding and/or grain boundary diffusion may play an important role in the creep of pillars, which is in agreement with our findings through estimations of stress exponent and activation volume (to be discussed in Section 4.1).

3.2. Engineering stress-strain curves

In Fig. 2(a), representative curves (for diameter $d = \sim 600$ nm) of load (P) vs. displacement (h) obtained from creep experiments are provided. From the recorded P–h data, the engineering stress (σ) and engineering strain (ε) in Fig. 2(b) were calculated as $\sigma \sim P/[\pi\ (d/2)^2]$ and $\varepsilon \sim h/l_0$, respectively, where l_0 is the initial height of pillar and the pillar diameter d was empirically determined as the diameter measured at ~30% of the pillar height from the pillar top for considering tapering effect. Overlapping of the loading portion of the curves in a single line indicates that the stress applied at the onset of creep is within the nominal elastic strain regime.

Important feature in the figure is that the creep indeed occurs at room temperature, and exhibits a displacement up to ~20 nm (for 200 s load-holding) at stresses well below the nominal yield strength of the pillars (~1.2–1.5 GPa, measured through uniaxial compression). The total amount of creep strain at holds is found to significantly increase with the applied stress in the range of $\sim 2 \times 10^{-4}$–9×10^{-3}. This stress-dependency of the creep strain indicates that the observed creep behavior is not an artifact caused by thermal drift which does not depend on load and thus stress (Yoo et al., 2012). Note again that previous nanoindentation creep tests with a sharp indenter were made in the plastic strain regime, which may differ from the conventional uniaxial creep tests under stresses below the nominal yield stress. One can gain a hint for this low-stress RT creep from some early works in the literature suggesting that the microscopic/incipient plasticity in nanostructured materials occurs at a stress level that is well below (often <50% of) their macroscopic yield stress (e.g., see Wang et al., 2007).

3.3. Creep curves

Fig. 3 provides representative examples of creep strain, ε_{creep}, vs. holding time, t, plots. The curves are mostly parabolic in nature, which is similar to the typical high-temperature creep curve of metals and alloys (Dieter, 1988; Kassner and Pérez-Prado, 2004); the creep curves consist of two regimes in the early stages: transient (primary) creep regime and steady-state (secondary) creep. It is clear that a large portion of creep strain was produced in primary creep regime. In addition to the

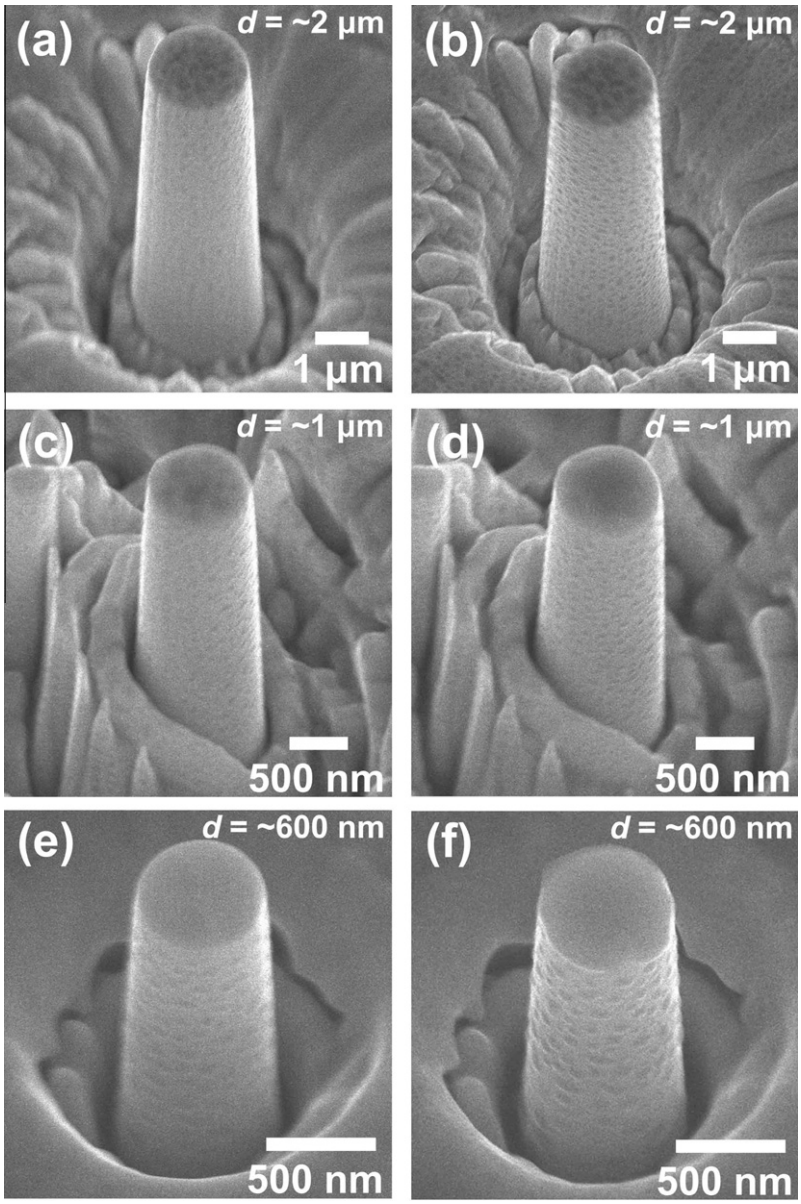

Fig. 1. Representative SEM images of pillar before (a), (c), (e) and after (b), (d), (f) the creep test at σ = 1000 MPa; (a), (b) for 2000 nm, (c), (d) for 1000 nm, and (e), (f) for 600 nm. Note the magnification disparity of each image.

stress-dependency of creep strain mentioned in previous section, this two-regime behavior also supports our suggestion that the creep is not caused by thermal drift, because thermal drift is expected to induce approximately a linear relation between strain and time instead of this two-regime relation. Note that, in Fig. 3, a large portion of creep strain is produced in early stage of creep or within 50–100 s (i.e., in primary creep regime).

The influences of d and σ on the creep amount are summarized in Fig. 4(a) where the total creep strain, $\varepsilon_{\text{total}}$, is plotted as a function of d. For clarity, the results obtained with the lowest and highest stress (400 and 1000 MPa, respectively) are separately shown in the inset of the figure. Two trends are clear in the figure: First, for a given σ, $\varepsilon_{\text{total}}$ increases with decreasing d. Second, for a given d, $\varepsilon_{\text{total}}$ increases with increasing σ.

While only the change in engineering creep strain (that is, the creep displacement divided by pillar height) is shown in Fig. 4(a), one can argue that the size effect in Fig. 4(a) is possibly a drift-induced artifact because the same amount of thermal drift will lead to higher creep strain for a pillar having smaller height. However, this hypothesis can be ruled out by Fig. 4(b) where not only the strain but the net value of total creep displacement is also significantly affected by d and σ in the same manner. Thus, Fig. 4(b) suggests that, while the absolute values of the creep strain reported here can be somewhat affected by the thermal drift, the observed size effect (i.e., smaller pillars have higher creep strain) is realistic.

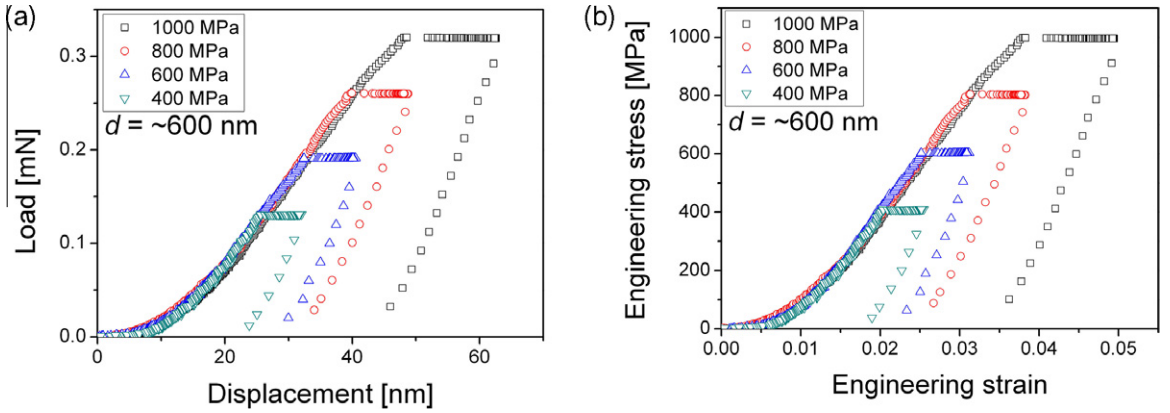

Fig. 2. Representative data from uniaxial compression pillar creep experiments (for d = ~600 nm); (a) load vs. displacement curves, and (b) engineering stress vs. engineering strain curves.

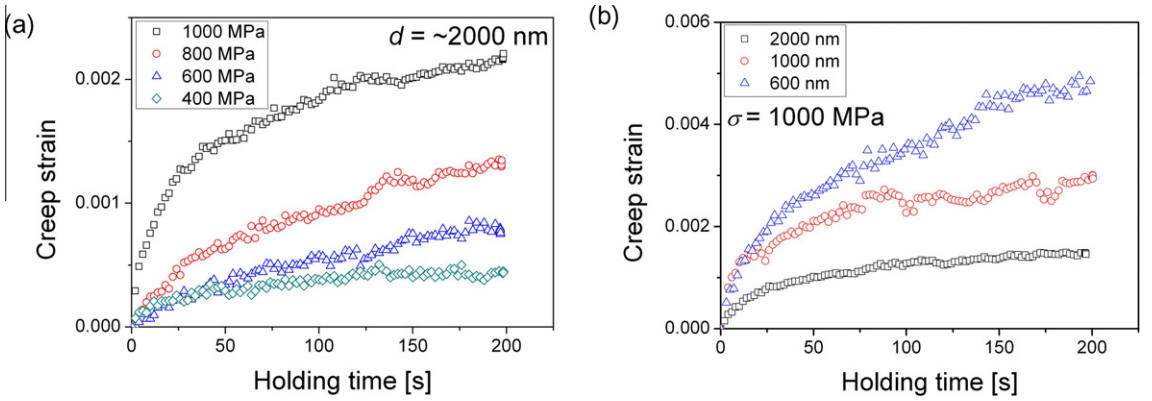

Fig. 3. Examples of creep strain vs. time curve: (a) effect of the applied stress; (b) effect of the pillar size.

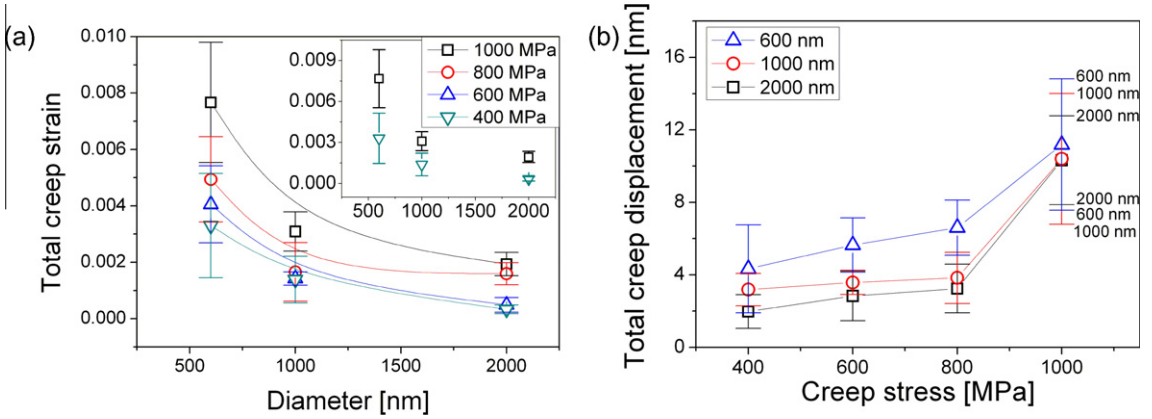

Fig. 4. Effects of d and σ on the total creep amount; (a) the total creep strain vs. d (for clarity, the cases at 400 and 1000 MPa are shown separately in the inset figure), and (b) the total creep displacement vs. σ.

3.4. Creep rate curves

The steady-state creep strain rate $\dot{\varepsilon}$ in Eq. (1) is an important quantitative measure of the creep behavior (Dieter, 1988; Kassner and Pérez-Prado, 2004). Here, the $\dot{\varepsilon}$ was estimated by fitting the creep curves (in Fig. 3) according to Garofalo's mathematical fitting equation originally suggested for conventional tensile creep analysis (Dieter, 1988):

$$\varepsilon_{creep} = \varepsilon_0 + \alpha(1 - e^{-rt}) + \omega t \quad (2)$$

where ε_0 is an instantaneous strain during loading (which is 0 here; see Fig. 3), and α, ω, r are creep constants: physical meaning of α and ω may be the limit of transient creep strain and the steady-state creep rate, respectively, and r is the ratio of transient creep rate to the transient creep strain. By differentiating Eq. (2) with respect to t, the logarithmic change in $\dot{\varepsilon}$ was obtained as a function of time or creep strain. Typical examples are provided in Fig. 5(a) and (b) for the same data of $d \sim 2000$ nm, suggesting the possibility of close approach to the steady-state condition, although it is theoretically implausible to reach the steady-state condition during short holding time (200 s). Note that the 'quasi-steady-state' strain rates ($\sim 10^{-6}$–10^{-5} s^{-1}) we observed here is higher than those in conventional uniaxial experiments (Wang et al., 1997; Yin et al., 2001). Fig. 5(c) summarizes the variation in quasi-steady-state strain rate (determined as the $\dot{\varepsilon}$ value at t = 200 s) with both d and σ. Similar to the trends in Fig. 4(a), higher $\dot{\varepsilon}$ is clear for smaller d and higher σ.

4. Discussion

4.1. Stress exponent, activation volume, and creep mechanism

Estimating the dominant creep mechanism is essential for better understanding the nanoscale viscoplasticity of nc-Ni. A useful indicator for the dominant creep mechanism is the creep stress exponent n ($=\frac{\partial \log \dot{\varepsilon}}{\partial \log \sigma}$) of Eq. (1); i.e., n = 1 for diffusion creep such as Nabarro–Herring creep (by lattice diffusion) and Coble creep (by grain boundary diffusion), n = 2 for grain boundary sliding, and n = 3–8 for dislocation creep (Dieter, 1988; Kassner and Pérez-Prado, 2004). Fig. 6 shows the logarithmic changes in steady-state strain rate with the applied stress, where the stress exponent n can be calculated from a slope of $\log(\dot{\varepsilon})$ and $\log(\sigma)$. From a linear fitting of only the 'average points,' the n is determined as 1 for $d = \sim 600$ nm, 1.13 for $d = \sim 1000$ nm, and 1.89 for $d = \sim 2000$ nm. However, it is difficult to deterministically state that the stress exponent

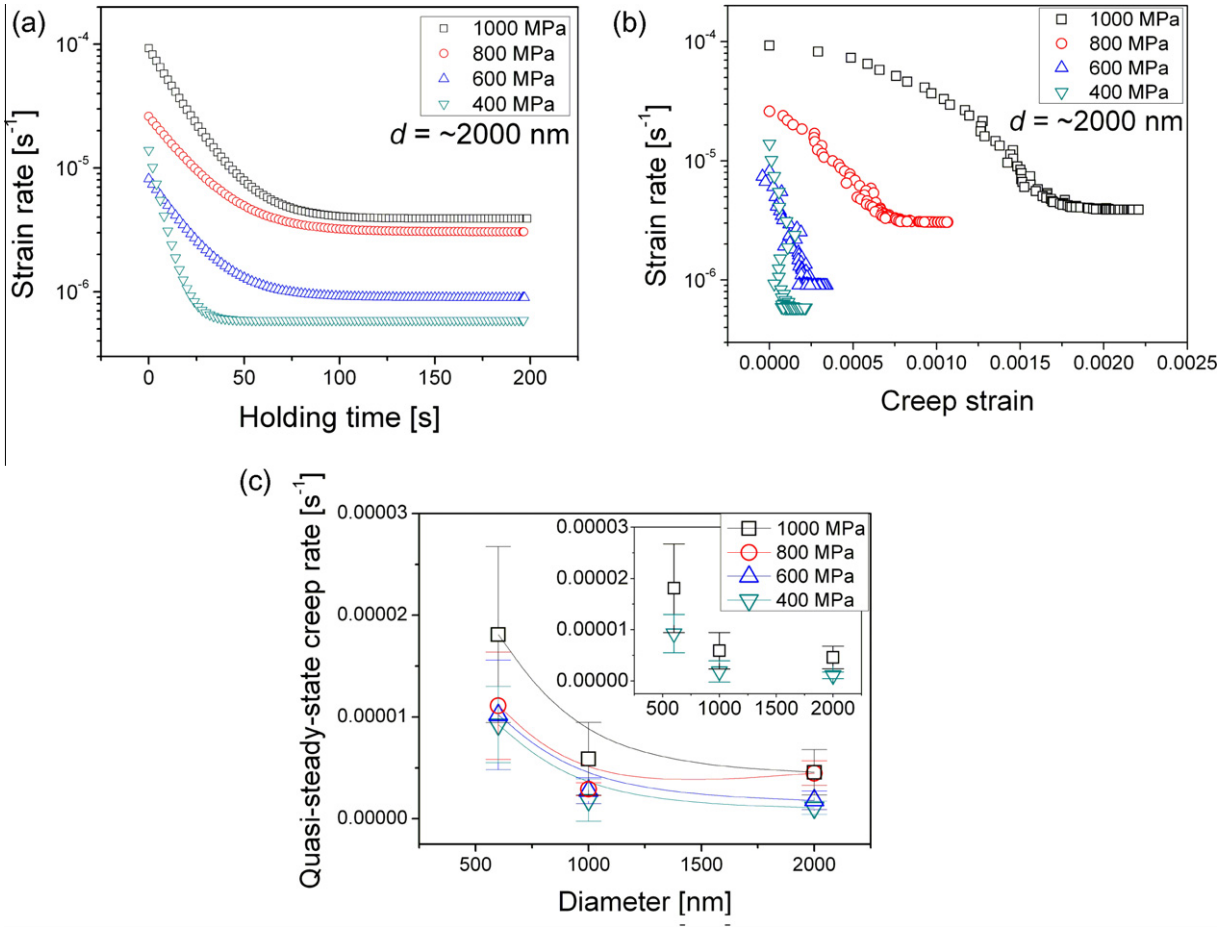

Fig. 5. Representative results of strain rate; (a) typical example (for $d = \sim 2000$ nm) of logarithmic creep strain rate vs. time; (b) logarithmic creep rate vs. creep strain, which is converted from (a); (c) variation in the quasi-steady-state creep strain rate as a function of pillar diameter (with inset figure showing the cases at 400 and 1000 MPa).

decreases with reducing pillar diameter because there is the data fluctuation as shown in Fig. 6 and thus the exponent can vary by selecting different points. It may be more reasonable to say that the stress exponent is in the range of 1–2.

To compare our results with the stress vs. strain rate relations in the literature, we summarize the creep stress exponent n and strain rate sensitivity $\left(\mathrm{SRS}, m = \frac{\partial \log \sigma}{\partial \log \dot{\varepsilon}}\right)$ data of nc-Ni obtained from various experiments (see Table 1). All nc-Ni samples listed in the table were prepared by either electrodeposition (ED) or pursed ED process (the latter case is marked with *). As seen in the table, (to our best knowledge) only two original papers (Wang et al., 1997; Yin et al., 2001) reported the RT creep stress exponent of nc-Ni through conventional uniaxial tensile creep experiments. At RT, Wang et al. (Wang et al., 1997) reported $n = \sim 1.18$ for the grain size d of 6 nm, $n = \sim 2$ for both $d = 20$ and 40 nm (low stress case), and $n = \sim 5.3$ for $d = 40$ nm (high stress case), while Yin et al. (Yin et al., 2001) found $n = \sim 1.1$ for 30 nm-sized nc-Ni. The n value (1–2) from our pillar creep tests of 30 nm-sized sample under stresses below nominal yielding stress is similar to these data, which suggests that the low-stress-induced creep in the present study is likely dominated by diffusion-controlled mechanisms such as GB sliding and GB diffusion rather than the dislocation activities. Note that, despite similar n, the strain rates in Fig. 6 ($\sim 10^{-6}$–10^{-5}) is much higher than $\sim 10^{-9}$–10^{-8} in the literature (Wang et al., 1997; Yin et al., 2001), which may be partly due to the difference in loading type and the imperfect pillar geometry for uniaxial loading (such as small taper of $\sim 3^{\circ}$), but mostly due to sample size effect (as expected from Fig. 4(a)). We will revisit this issue in the following section.

It is noteworthy that the n of Eq. (1) has been often estimated from the SRS (m of $\sigma = K(\dot{\varepsilon})^m$ which is obtained through either multiple uniaxial tests at various strain rates or strain-rate-jump tests) by simple conversion, $n = 1/m$. However, we notice that there can be two critical issues arising from such simplified conversion. First, mechanical environments for determining n and m are seriously different from each other. As the definition of m is $\left(\frac{\partial \log \sigma}{\partial \log \dot{\varepsilon}}\right)_{\varepsilon,T}$, the key data are the change in 'stress' measured at a given 'strain' and temperature. Although equations look similar, however, the $n = \left(\frac{\partial \log \dot{\varepsilon}}{\partial \log \sigma}\right)_{\sigma,T}$ is obtained from uniaxial creep tests where the change in 'strain' is monitored at a given 'stress' and temperature. Second and more importantly, there is the serious difference in applied stress level; the SRS tests are conducted at plastic stress regime, but conventional creep tests are performed well before the macroscopic yielding point (as in the present work). This difference in stress level could conceivably result in different deformation mechanism.

Another important clue for the creep mechanism can be gained by analyzing the activation volume of the event. Since the creep behavior is a thermally activated process regardless of its mechanism, the strain-rate dependency of the nanoscale creep event in Eq. (1) can be re-described in a simple Boltzmann form:

$$\dot{\gamma} = \dot{\gamma}_0 \times \exp\left(-\frac{\Delta G^*}{kT}\right) = \dot{\gamma}_0 \times \exp\left(-\frac{\Delta F^* - \tau V^*}{kT}\right) \tag{3}$$

where ΔG^* is the Gibbs free energy of activation, $\dot{\gamma}_0$ is the attempt frequency, ΔF^* and V^* are the Helmholtz activation free energy and activation volume of the event, respectively, and τ is the applied shear stress acting on V^*. From this equation with the von Mises yield criterion, the activation volume can be estimated as

$$V^* = \sqrt{3}kT\left(\frac{\partial \ln \dot{\varepsilon}}{\partial \sigma}\right) = \frac{\sqrt{3}nkT}{\sigma} \tag{4}$$

showing that high n can be related with large V^*. By employing the representative n from 'average' data points in Fig. 6 (i.e., $n = 1$, 1.13, and 1.89 for 600, 1000, 2000 nm, respectively), the V^* is calculated, and is shown in Table 2 normalized to the cube of Burgers vector of nickel ($b = 0.249$ nm). In Table 2, the V^* increases in the range of 0.5–$2.2b^3$ with decreasing stress

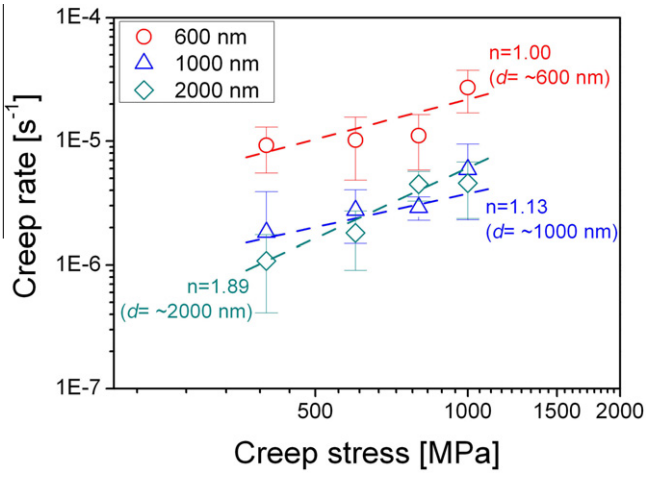

Fig. 6. Strain rate vs. stress relation to estimate the stress exponent n.

Table 1
Stress exponent and strain rate sensitivity measured from various tests. The samples were prepared by either electrodeposition or pulsed electrodeposition (in the studies marked with *). (T, tension; C, compression; I, indentation; GBA, grain boundary activities including GB sliding, GB migration, GB rotation and/or GB diffusion; DC, dislocation creep including glide and climb.)

d (nm)	T (K)	Testing method	Stress (GPa)	Strain rate (s^{-1})	n	m	Mechanism	Ref.
30	RT	C	0.4–1.0	$\sim10^{-6}$–10^{-5}	1.0–2.0		GBA	This study
6	RT	T	0.5–1.0	$\sim10^{-6}$–10^{-7}	1.18		GBA	Wang et al. (1997)
20	RT	T	0.5–1.2	$\sim10^{-9}$–10^{-8}	2		GBA	Wang et al. (1997)
40	RT	T	0.5–1.2	$\sim10^{-10}$–10^{-8}	2 5.3		DC	Wang et al. (1997)
30	RT	T	0.5–1.05	$\sim10^{-9}$	1.1		GBA	Yin et al. (2001)*
20	RT	T	1.4–2.6	$\sim10^{-5}$–10^{-2} $\sim10^{3}$		0.01–0.03 0.47	–	Dalla Torre et al. (2002)
30	77, RT	T	1–1.15			0.02	DC	Wang and Ma (2004)*
21	RT	T	0.8–2.0	$\sim10^{-5}$–10^{-4}		0.015–0.035	DC	Dalla Torre et al. (2005)
37	RT	T	1.2–2.0	$\sim10^{-6}$–10^{0}		0.016–0.045	DC	Shen et al. (2008)
20	RT	C	2.0–2.4	$\sim10^{-3}$–10^{-2}		0.02–0.03	GBA	Pan et al. (2007)
25	RT, 373	C	1.3–1.7	$\sim10^{-5}$–10^{-3}	8–100		DC	Blum and Li (2007)*
25	RT-474	C	1.5–1.7	$\sim10^{-5}$–10^{-3}		0.01–0.05	DC	Li et al. (2007)*
80	RT-474	C	0.8–1.1	$\sim10^{-6}$–10^{-3}		0.009–0.06	DC	Li et al.,(2007)*
20	RT	I	1.7–2.0	$\sim10^{-3}$–10^{-1}		0.033	DC	Gu et al. (2007)
		T	1.5–1.9	$\sim10^{-5}$–10^{-1}		0.016		
25	RT	I	1.8–3.8	$\sim10^{-2}$–10^{-4}	20–140		GBA, DC	Ma et al. (2008a)
30	RT	I	0.4–0.9	$\sim10^{-8}$	1.02–1.85		GBA	Choi et al. (2011)
25	RT	I	1.4–1.8	$\sim10^{-4}$–10^{-2}		0.019	DC	Maier et al. (2011)*
19	573–777	T	0.01–0.1	$\sim10^{-3}$–10^{0}		~0.8	GBA	Prasad and Chokshi (2010)
30	373	T	0.5–1.05	$\sim10^{-7}$–10^{-8}	6.5		DC	Yin et al. (2001)*
15	77–363	T	0.9–1.5	$\sim10^{-8}$		0.0025–0.035	DC	Wang et al. (2006)
40	373	C	1.0–2.0	$\sim10^{-8}$–10^{-4}	8–12		GBA, DC	Kottada and Chokshi (2005)
60	398	I	1.3–1.8	$\sim10^{-2}$–10^{-3}	5.78		DC	Wang et al. (2010)
		C	1.3–1.8	$\sim10^{-4}$–10^{-5}	5.13			
44–77	348, 398, 448	I	0.6–2.0	$\sim10^{-3}$	3.11–14.81		DC	Wang et al. (2009)

Table 2
The activation volumes estimated for different stress and pillar size. (b = 0.249 nm.)

Creep stress (MPa)	Diameter (nm)		
	600	1000	2000
400	$1.15b^3$	$1.30b^3$	$2.18b^3$
600	$0.77b^3$	$0.87b^3$	$1.45b^3$
800	$0.58b^3$	$0.65b^3$	$1.09b^3$
1000	$0.46b^3$	$0.52b^3$	$0.87b^3$

and increasing pillar size. While the stress-dependency can be expected from Eq. (4), the increasing volume with the pillar size may not have physical meaning because the volumes in Table 2 are calculated using average n values without consideration of possible fluctuation we mentioned earlier. However, if this trend of size-dependency holds valid, it may be partly explained by the uniform deformation of the pillar observed in SEM images of Fig. 1; i.e., the deforming volume for the time-dependent plasticity is proportional to the volume of a pillar.

The most important feature in the data is that the estimated V^* is mostly less than $2b^3$ or sometimes close to one atomic volume ($\sim b^3$), which may suggest the mechanisms of GB diffusion, i.e., GB sliding or even Coble creep (Wang et al., 2006). These V^*s are certainly much smaller than those estimated from SRS test of nc-Ni at RT, $\sim10b^3$ (Wang et al., 2006), corresponding to the dislocation-mediated flow, and instead, somewhat close to those for the nanoindentation-induced heterogeneous nucleation of dislocations in a metal ($\sim0.5b^3$) where vacancy can play a significant role (Schuh et al., 2005). In addition to the n estimation (i.e., $\leqslant2$), the V^* calculation may support that the low-stress-induced creep deformation at RT here is dominated by diffusion-controlled mechanisms instead of dislocation creep. The different V^* of this work from the previous SRS experiments may be due to the different stress level in a similar way as we explained the difference in the n and m above. The general picture of low-stress creep mechanism in the present study is in an agreement with an expectation from deformation mechanism maps for nc-Ni (constructed in terms of stress vs. temperature (Wang et al., 1997) or stress vs. grain size (Mohamed, 2011)) of which GB-mediated deformation mechanism including GB sliding, GB migration, GB rotation, or Coble creep is preferred in the target regime. We note again, however, that the creep strain rate observed in

our experiments (10^{-6}–10^{-5} s^{-1}) is substantially higher than those previously reported for RT creep of nc-Ni, 10^{-9}–10^{-8} s^{-1} (Gruen, 1999; Sherby and Wadsworth, 1989), which implies that the diffusion-controlled mechanisms seen in our experiments may be different from conventional mechanisms of Coble creep and GB sliding. Despite certain limitations of the microcompression creep experiments (e.g., thermal drift and quasi-steady-state approach), the free surface (a special interface) in our pillars appear to conceivably play a role in enhancing the creep strain rate (to be discussed in the following section).

4.2. Pillar size effect on the nanoscale creep

The above observation implies that the creep behavior is more pronounced for a smaller pillar; total creep strain (Fig. 4(a)) and steady-state-like strain rate (Fig. 5(c)) dramatically increases with reducing pillar size. This trend becomes clearer if the data are compared with bulk data. For example, as mentioned above, the strain rates in the present study ($\sim 10^{-6}$–10^{-5}) is much higher than those from bulk test at RT, $\sim 10^{-9}$–10^{-8} (Wang et al., 1997; Yin et al., 2001), although the n values are similar. Our data is also higher than theoretical values for GBS and Coble creep that can be calculated as (Coble, 1963; Lüthy et al., 1979)

$$\dot{\varepsilon}_{\mathrm{GBS}} = 2 \times 10^{5} D_{\mathrm{GB}} \frac{Gb}{kT} \left(\frac{b}{d}\right)^{3} \left(\frac{\sigma}{G}\right)^{2} \quad (\mathrm{in/s}) \tag{5}$$

$$\dot{\varepsilon}_{\mathrm{Coble}} = 148 \frac{\sigma \Omega \delta D_{\mathrm{GB}}}{\pi d^{3} kT} \quad (\mathrm{in/s}) \tag{6}$$

Since the GB diffusion coefficient D_{GB} can be given as (Frost and Ashby, 1982)

$$D_{\mathrm{GB}} \approx 4 \times 10^{-5} \exp\left(-\frac{66.4 T_{m}}{RT}\right) \quad (\mathrm{in\ m^2/s}) \tag{7}$$

it is possible to estimate the strain rates by putting proper values of the relevant parameters for nickel (atomic volume $\Omega = 1.09 \times 10^{-29}$ m^3, shear modulus $G = 78.9$ GPa, melting temperature $T_{\mathrm{m}} = 1726$ K, effective diffusive thickness of GB $\delta = 2b$), Boltzmann constant k and gas constant R into the equations. The calculated values are 4.6×10^{-9}–2.9×10^{-8} s^{-1} for GBS and 3×10^{-10}–7.5×10^{-10} s^{-1} for Coble creep. Therefore, it is obvious that there is a significant discrepancy between strain rate predicted for bulk case and the strain rate measured at the nanoscale; i.e., the measured values are much higher than predicted ones.

A pertinent question arising at this point is what is the physical phenomenon that leads to the enhanced creep in smaller pillars? A clue for the answer can be gained by considering the increased contribution of free surface in the pillar specimens vis-à-vis the bulk samples. The reason for the size effect in our hypothesis is two-fold. First possible cause for the size effect is based on the fact that the free surface itself is very effective diffusion path. Although the diffusivity of the so-called 'short circuit diffusion' along surface in a crystalline metal may vary depending on the crystallographic orientation, it is often approximated by summarizing the data in a random direction and given as (Gjostein, 1973; Gleiter and Chalmer, 1972; Nishizawa, 2008),

$$D_{\mathrm{surf}} \approx 7 \times 10^{-6} \exp\left(-\frac{56 T_{\mathrm{m}}}{RT}\right) \quad (\mathrm{in\ m^2/s}) \tag{8}$$

By putting $T_{\mathrm{m}} = 1726$ K and $T = 298$ K into Eqs. (7) and (8), we could estimate $D_{\mathrm{surf}} \approx 7.98 \times 10^{-23}$ m^2/s and $D_{\mathrm{GB}} \approx 3.26 \times 10^{-25}$ m^2/s for the bulk sample and thus the ratio of $D_{\mathrm{surf}}/D_{\mathrm{GB}}$ is higher than 200. This large ratio suggests that the surface (area)-to-volume ratio (SVR), can significantly affect the creep characteristics of the pillars. By assuming a perfect cylindrical geometry for the pillars, here the SVRs are calculated as 2.2×10^{-3}, 4.3×10^{-3} and 7.2×10^{-2} /nm for $d = \sim 2000$, 1000 and 600 nm, respectively. From this, one may expect that the rapid increase in SVR with reducing pillar size will drastically enhance creep strain and strain rate.

Second possibility (or to a much less extent) may be related to the previous suggestion that T_{m} of a nanomaterial having d of a few nanometer can decrease with increasing SVR (Ahmad and Murr, 1976; Couchman and Jesser, 1977; Goldstein et al., 1992; Guisbiers and Buchaillot, 2008). For the sake of completeness, we discuss this effect here. According to reference (Goldstein et al., 1992), the trend can be describable as

$$T_{\mathrm{m}} = T_{\mathrm{m,bulk}} \left[1 + \left(\frac{\gamma_{\mathrm{l}} - \gamma_{\mathrm{s}}}{\Delta H_{\mathrm{m,bulk}}}\right) \frac{A}{V}\right] \tag{9}$$

$T_{\mathrm{m,bulk}}$ is the T_{m} of bulk-scale, γ_{l} and γ_{s} is surface energy of liquid and solid respectively, $\Delta H_{\mathrm{m,bulk}}$ is bulk melting enthalpy, and A/V is the SVR. If Eq. (9) can be extrapolated to a bigger size (although low possibility), a 'slight' change in T_{m} is expected by reducing pillar size (i.e., increasing SVR). In consideration of the values for pure nickel ($\gamma_{\mathrm{l}} = 1.78$ J/m^2, $\gamma_{\mathrm{s}} = 2.05$ J/m^2 (Guisbiers and Buchaillot, 2008), and $\Delta H_{\mathrm{m,bulk}}$ is 17,470 J/mol), we could obtain the T_{m} of each pillar as 1722, 1718, 1713 K for diameter of 2000, 1000 and 600 nm, respectively. The decrease in T_{m} is indeed very small but could in principal lead to higher homologous temperature (T/T_{m}) where creep rate enhances. Alternatively, this can be understood in terms of

Table 3
The summary of calculated diffusivity for surface and grain boundary diffusion.

Diameter [nm]	T_m [K]	D_{surf} [m^2/s]	D_{GB} [m^2/s]
600	1713	1.07×10^{-22}	4.62×10^{-25}
1000	1718	9.53×10^{-23}	4.01×10^{-25}
2000	1722	8.72×10^{-23}	3.62×10^{-25}
Bulk	1726	7.98×10^{-23}	3.26×10^{-25}

creep activation energy; according to $Q = CT_m$ where Q is the activation energy and C is the material's constant independent of size, the creep activation energy in principal decreases with reducing T_m (but is clearly too small to consider). As mentioned above, the values of both D_{surf} and D_{GB} rapidly increase with reducing pillar size (and thus T_m), as listed in Table 3. For any case in the table, the ratio of D_{surf}/D_{GB} is higher than about 200, which could be the primary reason for a more pronounced creep behavior for a smaller pillar (having higher SVR). Finally but not surprisingly, we would like to point out that grain growth was not observed in our creep tested samples due to the low stresses in our experiment and impurities intrinsic to electrodeposited nc-Ni (Wang et al., 2012a). Therefore, the grain growth related mechanisms are not applicable to our discussions.

5. Conclusions

Low-stress-induced nanoscale creep of nc-Ni at RT was systematically explored through compression creep experiments performed on nano-/micro-pillars (having diameters of 600, 1000, and 2000 nm). It was revealed that the creep indeed occurs at ambient temperature and at the stresses that are well below the nominal yield stress of the pillars. The postmortem SEM analysis suggests that the creep deformation is uniform in nature. The total creep strain and quasi-steady-state creep strain are significantly affected by both the applied stress and the pillar size; i.e., with increasing stress or decreasing pillar diameter, the creep behavior was largely enhanced. Estimation of the stress exponent and the activation volume for the creep event suggests that the nanoscale RT creep at low stress (below nominal yield stress) may be dominated by diffusion-controlled mechanisms such as free surface assisted GB diffusion and GB sliding. The more pronounced creep plasticity for smaller pillar is rationalized in consideration of enlarged contributions of free surface at the pillar experiments.

Acknowledgements

This research was supported by Basic Science Research Program through the National Research Foundation of Korea (NRF) funded by the Ministry of Education, Science and Technology (No. 2010-0025526), and in part by the Human Resources Development of the Korea Institute of Energy Technology Evaluation and Planning (KETEP) grant funded by the Korea government Ministry of Knowledge Economy (No. 20114010203020). The work at Lawrence Livermore National Laboratory was performed under the auspices of the US Department of Energy under Contract DE-AC52-07NA27344.

References

Ahmad, U.M., Murr, L.E., 1976. Surface free energy of nickel and stainless steel at temperatures above the melting point. J. Mater. Sci. 11, 224–230.
Baghbanan, M., Erb, U., Palumbo, G., 2006. Towards the application of nanocrystalline metals in MEMS. Phys. Status Solidi A 203, 1259–1264.
Barai, P., Weng, G.J., 2009. Mechanics of very fine-grained nanocrystalline materials with contributions from grain interior, GB zone, and grain-boundary sliding. Int. J. Plasticity 25, 2410–2434.
Benkassem, S., Capolungo, L., Cherkaoui, M., 2007. Mechanical properties and multi-scale modeling of nanocrystalline materials. Acta Mater. 55, 3563–3572.
Blum, W., Li, Y.J., 2007. Flow stress and creep rate of nanocrystalline Ni. Scr. Mater. 57, 429–431.
Capolungo, L., Cherkaoui, M., Qu, J., 2007. On the elastic-viscoplastic behavior of nanocrystalline metals. Int. J. Plasticity 23, 561–591.
Chen, M.W., Ma, E., Hemker, K.J., Sheng, H., Wang, Y.M., Cheng, X., 2003. Deformation twinning in nanocrystalline aluminum. Science 300, 1275–1277.
Choi, I.-C., Yoo, B.-G., Kim, Y.-J., Seok, M.-Y., Wang, Y.M., Jang, J.-I., 2011. Estimating the stress exponent of nanocrystalline nickel: sharp vs. spherical indentation. Scr. Mater. 65, 300–303.
Choi, I.-C., Yoo, B.-G., Kim, Y.-J., Jang, J.-I., 2012. Indentation creep revisited. J. Mater. Res. 27, 3–11.
Cleri, F., 2012. A two-phase model of large-strain plasticity in covalent nanostructures. Int. J. Plasticity. http://dx.doi.org/10.1016/j.ijplas.2012.04.005.
Coble, R.L., 1963. A model for boundary diffusion controlled creep in polycrystalline materials. J. Appl. Phys. 34, 1679–1982.
Couchman, P.R., Jesser, W.A., 1977. Thermodynamic theory of size dependence of melting temperature in metals. Nature 269, 481–483.
Dalla Torre, F., Van Swygenhoven, H., Victoria, M., 2002. Nanocrystalline electrodeposited Ni: microstructure and tensile properties. Acta Mater. 50, 3957–3970.
Dalla Torre, F., Spätig, P., Schäublin, R., Victoria, M., 2005. Deformation behaviour and microstructure of nanocrystalline electrodeposited and high pressure torsioned nickel. Acta Mater. 53, 2337–2349.
Dao, M., Lu, L., Asaro, R.J., De Hosson, J.T.M., Ma, E., 2007. Toward a quantitative understanding of mechanical behavior of nanocrystalline metals. Acta Mater. 55, 4041–4065.
Dieter, G.E., 1988. Mechanical Metallurgy. McGraw-Hill, London.
Farrokh, B., Khan, A.S., 2009. Grain size, strain rate, and temperature dependence of flow stress in ultra-fine grained and nanocrystalline Cu and Al: synthesis, experiment, and constitutive modeling. Int. J. Plasticity 25, 715–732.
Frost, H.J., Ashby, M.F., 1982. Deformation-Mechanism Maps: The Plasticity and Creep of Metals Ceramics. Pergamon Press, Oxford.
Gianola, D.S., Van Petegem, S., Legros, M., Brandstetter, S., Van Swygenhoven, H., Hemker, K.J., 2006. Stress-assisted discontinuous grain growth and its effect on the deformation behavior of nanocrystalline aluminum thin films. Acta Mater. 54, 2253–2263.
Gjostein, N.A., 1973. ASM Seminar on Diffusion, ASM International, Metals Park, OH.

Gleiter, H., Chalmer, B., 1972. Grain-boundary diffusion. Prog. Mater. Sci. 16, 77–112.
Goldstein, A.N., Echer, C.M., Alivisatos, A.P., 1992. Melting in semiconductor nanocrystals. Science 256, 1425–1427.
Greer, J.R., Oliver, W.C., Nix, W.D., 2005. Size dependence of mechanical properties of gold at the micron scale in the absence of strain gradients. Acta Mater. 53, 1821–1830.
Gruen, D.M., 1999. Nanocrystalline diamond films. Annu. Rev. Mater. Sci. 29, 211–259.
Gu, C.D., Lian, J.S., Jiang, Q., Zheng, W.T., 2007. Experimental and modeling investigations on strain rate sensitivity of an electrodeposited 20 nm grain sized Ni. J. Phys. D: Appl. Phys. 40, 7440–7446.
Guisbiers, G., Buchaillot, L., 2008. Size and shape effects on creep and diffusion at the nanoscale. Nanotechnology 19, 435701.
Gusev, A.I., 1998. Effects of the nanocrystalline state in solids. Phys. Usp. 41, 49–76.
Han, B.Q., Lavernia, E., Mohamed, F.A., 2005. Mechanical properties of nanostructured materials. Rev. Adv. Mater. Sci. 9, 1–16.
Jang, D., Greer, J.R., 2011. Size-induced weakening and grain boundary-assisted deformation in 60 nm grained Ni nanopillars. Scr. Mater. 64, 77–80.
Johnson, K.L., 1985. Contact Mechanics. Cambridge University Press, Cambridge.
Kassner, M.E., Pérez-Prado, M.T., 2004. Fundamentals of Creep in Metals and Alloys. Elsevier, Oxford.
Khan, A.S., Suh, Y.S., Chen, X., Takacs, L., Zhang, H., 2006. Nanocrystalline aluminum and iron: mechanical behavior at quasi-static and high strain rates, and constitutive modeling. Int. J. Plasticity 22, 195–209.
Kim, J.-Y., Greer, J.R., 2009. Tensile and compressive behavior of gold and molybdenum single crystals at the nano-scale. Acta Mater. 57, 5245–5253.
Kottada, R.S., Chokshi, A.H., 2005. Low temperature compressive creep in electrodeposited nanocrystalline nickel. Scr. Mater. 53, 887–892.
Kumar, K.S., Suresh, S., Van Swygenhoven, H., 2003a. Mechanical behavior of nanocrystalline metals and alloys. Acta Mater. 51, 5743–5774.
Kumar, K.S., Suresh, S., Chisholm, M.F., Horton, J.A., Wan, P., 2003b. Deformation of electrodeposited nanocrystalline nickel. Acta Mater. 51, 387–405.
LaFontaine, W.R., Yost, B., Black, R.D., Li, C.-Y., 1990. Indentation load relaxation experiments with indentation depth in the submicron range. J. Mater. Res. 5, 2100–2106.
Li, J., Weng, G.J., 2007. A secant-viscosity composite model for the strain-rate sensitivity of nanocrystalline materials. Int. J. Plasticity 23, 2115–2133.
Li, Y.J., Mueller, J., Höppel, H.W., Göken, M., Blum, W., 2007. Deformation kinetics of nanocrystalline nickel. Acta Mater. 55, 5708–5717.
Lucas, B.N., Oliver, W.C., 1999. Indentation power-law creep of high purity indium. Metall. Mater. Trans. A 30A, 601–610.
Lüthy, H., White, R.A., Sherby, O.D., 1979. Grain boundary sliding and deformation mechanism maps. Mater. Sci. Eng. 39, 211–216.
Ma, Z.S., Long, S.G., Zhou, Y.C., Pan, Y., 2008a. Indentation scale dependence of tip-in creep behavior in Ni thin films. Scr. Mater. 59, 195–198.
Ma, Z., Long, S., Pan, Y., Zhou, Y., 2008b. Loading rate sensitivity of nanoindentation creep in polycrystalline Ni films. J. Mater. Sci. 43, 5952–5955.
Maier, V., Durst, K., Mueller, J., Backes, B., Höppel, H.W., Göken, M., 2011. Nanoindentation strain-rate jump tests for determining the local strain-rate sensitivity in nanocrystalline Ni and ultrafine-grained Al. J. Mater. Res. 26, 1421–1430.
Malygin, G.A., 2007. Plasticity and strength of micro- and nanocrystalline materials. Phys. Solid State 49, 1013–1033.
Mayo, M.J., Nix, W.D., 1988. A micro-indentation study of superplasticity in Pb, Sn, and Sn-38 wt% Pb. Acta Metall. 36, 2183–2192.
Mayo, M.J., Siegel, R.W., Narayanasamy, A., Nix, W.D., 1990. Mechanical properties of nanophase TiO_2 as determined by nanoindentation. J. Mater. Res. 5, 1073–1082.
McFadden, S.X., Mishra, R.S., Valiev, R.Z., Zhilyaev, A.P., Mukherjee, A.K., 1999. Low-temperature superplasticity in nanostructured nickel and metal alloys. Nature 398, 684–686.
Meredith, C.S., Khan, A.S., 2012. Texture evolution and anisotropy in the thermo-mechanical response of UFG Ti processed via equal channel angular pressing. Int. J. Plasticity 30–31, 202–217.
Meyer, M.A., Mishra, A., Benson, D.J., 2006. Mechanical properties of nanocrystalline materials. Prog. Mater. Sci. 51, 427–556.
Mohamed, F.A., 2011. Deformation mechanism maps for micro-grained, ultrafine-grained, and nano-grained materials. Mater. Sci. Eng. A 528, 1431–1435.
Nishizawa, T., 2008. Thermodynamics of Microstructures, ASM International, Materials Park, OH.
Ovid'ko, I.A., 2005. Deformation and diffusion modes in nanocrystalline materials. Int. Mater. Rev. 50, 65–82.
Pan, D., Kuwano, S., Fujita, T., Chen, M.W., 2007. Ultra-large room-temperature compressive plasticity of a nanocrystalline metal. Nano. Lett. 7, 2108–2111.
Pharr, G.M., Herbert, E.G., Gao, Y., 2010. The indentation size effect: A critical examination of experimental observations and mechanistic interpretation. Annu. Rev. Mater. Res. 40, 271–292.
Prasad, M.J.N.V., Chokshi, A.H., 2010. Superplasticity in electrodeposited nanocrystalline nickel. Acta Mater. 58, 5724–5736.
Rupert, T.J., Gianola, D.S., Gan, Y., Hemker, K.J., 2009. Experimental observations of stress-driven grain boundary migration. Science 326, 1686–1690.
Schuh, C.A., Mason, J.K., Lund, A.C., 2005. Quantitative insight into dislocation nucleation from high-temperature nanoindentation experiments. Nat. Mater. 4, 617–621.
Schwaiger, R., Moser, B., Dao, M., Chollacoop, N., Suresh, S., 2003. Some critical experiments on the strain-rate sensitivity of nanocrystalline nickel. Acta Mater. 51, 5159–5172.
Schwaiger, R., Weber, M., Moser, B., Gumbsch, P., Kraft, O., 2012. Mechanical assessment of ultrafine-grained nickel by microcompression experiment and finite element simulation. J. Mater. Res. 27, 266–277.
Shan, Z., Stach, E.A., Wiezorek, J.M.K., Knapp, J.A., Follstaedt, D.M., Mao, S.X., 2004. Grain boundary–mediated plasticity in nanocrystalline nickel. Science 305, 654–657.
Shen, X., Lian, J., Jiang, Z., Jiang, Q., 2008. High strength and high ductility of electrodeposited nanocrystalline Ni with a broad grain size distribution. Mater. Sci. Eng. A 487, 410–416.
Sherby, O.D., Wadsworth, J., 1989. Superplasticity and its applications. Prog. Mater. Sci. 33, 169–221.
Stone, D.S., Jakes, J.E., Puthoff, J., Elmustafa, A.A., 2010. Analysis of indentation creep. J. Mater. Res. 25, 611–621.
Suryanarayana, C., 2005. Recent developments in nanostructured materials. Adv. Eng. Mater. 7, 983–992.
Tjong, S.C., Chen, H., 2004. Nanocrystalline materials and coatings. Mater. Sci. Eng., R 45, 1–88.
Tucker, G.J., McDowell, D.L., 2011. Non-equilibrium grain boundary structure and inelastic deformation using atomistic simulations. Int. J. Plasticity 27, 841–857.
Uchic, M.D., Dimiduk, D.M., Florando, J.N., Nix, W.D., 2004. Sample dimensions influence strength and crystal plasticity. Science 305, 986–989.
Valiev, R.Z., Islamgaliev, R.K., Alexandrov, I.V., 2000. Bulk nanostructured materials from severe plastic deformation. Prog. Mater. Sci. 45, 103–189.
Valiev, R., 2004. Nanostructuring of metals by severe plastic deformation for advanced properties. Nat. Mater. 3, 511–516.
Van Swygenhoven, H., Derlet, P.M., Hasnaoui, A., 2002a. Atomic mechanism for dislocation emission from nanosized grain boundaries. Phys. Rev, B 66, 024101.
Van Swygenhoven, H., 2002. Grain boundaries and dislocations. Science 296, 66–67.
Wadsworth, J., Ruano, O.A., Sherby, O.D., 2002. Denuded zones, diffusional creep, and grain boundary sliding. Metall. Mater. Trans. A 33A, 219–229.
Wang, N., Wang, Z.R., Aust, K.T., Erb, U., 1997. Room temperature creep behavior of nanocrystalline nickel produced by an electrodeposition technique. Mater. Sci. Eng. A 237, 150–158.
Wang, Y.M., Chen, M., Zhou, F., Ma, E., 2002. High tensile ductility in a nanostructured metal. Nature 419, 912–915.
Wang, Y.M., Ma, E., 2004. On the origin of ultrahigh cryogenic strength of nanocrystalline metals. Appl. Phys. Lett. 85, 2750–2752.
Wang, Y.M., Hamza, A.V., Ma, E., 2006. Temperature-dependent strain rate sensitivity and activation volume of nanocrystalline Ni. Acta Mater. 54, 2715–2726.
Wang, Y.M., Hamza, A.V., Barbee, T.W., 2007. Incipient plasticity in metallic glass modulated nanolaminates. Appl. Phys. Lett. 91, 061924.
Wang, C.L., Zhang, M., Nieh, T.G., 2009. Nanoindentation creep of nanocrystalline nickel at elevated temperatures. J. Phys. D: Appl. Phys. 42, 115405.
Wang, C.L., Lai, Y.H., Huang, J.C., Nieh, T.G., 2010. Creep of nanocrystalline nickel: A direct comparison between uniaxial and nanoindentation creep. Scr. Mater. 62, 175–178.

Wang, Y.M., Ott, R.T., van Buuren, T., Willey, T.M., Biener, M.M., Hamza, A.V., 2012a. Controlling factors in tensile deformation of nanocrystalline cobalt and nickel. Phys. Rev. B 85, 014101.
Wang, B., Idrissi, H., Galceran, M., Colla, M.S., Turner, S., Hui, S., Raskin, J.P., Pardoen, T., Godet, S., Schryvers, D., 2012b. Advanced TEM investigation of the plasticity mechanism in nanocrystalline freestanding palladium films with nanoscale twins. Int. J. Plasticity 37, 140–156.
Wolf, D., Yamakov, V., Phillpot, S.R., Mukherjee, A.K., Gleiter, H., 2005. Deformation of nanocrystalline materials by molecular-dynamics simulation: relationship to experiments? Acta Mater. 53, 1–40.
Yamakov, V., Wolf, D., Phillpot, S.R., Mukherjee, A.K., Gleiter, H., 2004. Deformation-mechanism map for nanocrystalline metals by moleculardynamics simulation. Nat. Mater. 3, 43–47.
Yin, W.M., Whang, S.H., Mirshams, R., Xiao, C.H., 2001. Creep behavior of nanocrystalline nickel at 290 and 373 K. Mater. Sci. Eng. A 301, 18–22.
Yoo, B.-G., Kim, K.-S., Oh, J.-H., Ramamurty, U., Jang, J.-I., 2010a. Room temperature creep in amorphous alloys: influence of initial strain and free volume. Scr. Mater. 63, 1205–1208.
Yoo, B.-G., Oh, J.-H., Kim, Y.-J., Park, K.-W., Lee, J.-C., Jang, J.-I., 2010b. Nanoindentation analysis of time-dependent deformation in as-cast and annealed CueZr bulk metallic glass. Intermetallics 18, 1898–1901.
Yoo, B.-G., Kim, J.-Y., Kim, Y.-J., Choi, I.-C., Shim, S., Tsui, T.Y., Bei, H., Ramamurty, U., Jang, J.-I., 2012. Increased time-dependent room temperature plasticity in metallic glass nanopillars and its size-dependency. Int. J. Plasticity 37, 108–118.
Zhang, K., Weertman, J.R., Eastman, J.A., 2004. The influence of time, temperature, and grain size on indentation creep in high-purity nanocrystalline and ultrafine grain copper. Appl. Phys. Lett. 85, 5197–5199.
Zhu, T., Li, J., 2010. Ultra-strength materials. Prog. Mater. Sci. 55, 710–757.
Zhu, L., Lu, J., 2012. Modelling the plastic deformation of nanostructured metals with bimodal grain size distribution. Int. J. Plasticity 30–31, 166–184.